

Nanoporous $\text{Li}_3\text{V}_2(\text{PO}_4)_3/\text{C}$ microspheres with enhanced lithium ion diffusion for high-rate and long-life lithium ion batteries

Yanzhu Luo^a, Xu Xu^a, Yuxiang Zhang^b, Yuqiang Pi^b, Chunhua Han^{a,*}, Mengyu Yan^a, Qiulong Wei^a, Liqiang Mai^{a,*}

^a State Key Laboratory of Advanced Technology for Materials Synthesis and Processing, WUT-Harvard Joint Nano Key Laboratory, Wuhan University of Technology, Wuhan 430070, P. R. China

^b WUT Powerful Energy Co., Ltd., Wuhan 430223, P. R. China

*Authors for correspondence: Liqiang Mai, email: mlq518@whut.edu.cn

Chunhua Han, email: hch5927@whut.edu.cn

Received 29 Jun 2014; Accepted 01 Sep 2014; Available Online 01 Sep 2014

Abstract

Nanoporous lithium vanadium phosphate/carbon ($\text{Li}_3\text{V}_2(\text{PO}_4)_3/\text{C}$) microspheres assembled by well-crystalline nanoparticles in carbon matrix are synthesized by the decomposition of the microflower precursor. This nanoporous $\text{Li}_3\text{V}_2(\text{PO}_4)_3/\text{C}$ microspheres exhibit a specific surface area of 61.9 m^2/g and rich hierarchical pores, which makes the easy access of electrolyte to the active material to enhance the Li ion diffusion. When cycled at the rate of 10^o C, an initial specific capacity of 112 mAh/g can be obtained and the capacity retention reaches 88% after 500 cycles. Even after 2000 cycles, the retention is 77%, corresponding to the capacity fading of 0.014% per cycle. The stable capacity and excellent rate capability make nanoporous $\text{Li}_3\text{V}_2(\text{PO}_4)_3/\text{C}$ microsphere a promising cathode for lithium ion batteries.

Keywords: Nanoporous microspheres; Lithium vanadium phosphate; High-rate; Long-life; Li ion diffusion

1. Introduction

Due to environmental considerations, it is urgent to further prompt the development of electric vehicles (EVs) and hybrid electric vehicles (HEVs). Based on this requirement, batteries with high energy and power, long lifespan, low cost, environmental compatibility, and intrinsic thermal safety are urgently needed [1-8]. In recent years, the monoclinic lithium vanadium phosphate ($\text{Li}_3\text{V}_2(\text{PO}_4)_3$) has attracted considerable interest as a commercial lithium ion battery (LIB) cathode candidate for its thermodynamically stable structure, high cell-voltage and fairish theoretical specific capacity (133 mAh/g for extraction of two lithium ions between 3.0-4.3 V vs. Li/Li^+) [9-11]. More importantly, the $(\text{PO}_4)^{3-}$ polyanions provide a three dimensional pathway for Li^+ insertion/extraction, which results in a very high Li ion diffusion coefficient (from 10^{-9} to 10^{-10} cm^2/s), much higher than that of LiFePO_4 (from 10^{-14} to 10^{-16} cm^2/s) [12-15].

In order to improve the rate capabilities of electrode material, various strategies have been proposed, such as downsizing particle size, carbon coating, fabricating porous micro/nanostructures, etc. [16-21]. All the efforts are made to obtain the electrode materials with fast transfer of both electrons and Li ions. As mentioned above, $\text{Li}_3\text{V}_2(\text{PO}_4)_3$ has a very high Li ion diffusion coefficient. However, the structure and morphology will significantly influence this value, including the porosity, crystallinity, crystallite size, etc. Well-crystalline $\text{Li}_3\text{V}_2(\text{PO}_4)_3$ nanoparticles embedded into a carbon matrix with porous structure would be crucial to take full advantage of the fast Li ion diffusion of this material. Moreover, the continuous carbon matrix would also be beneficial for improving the low intrinsic electronic conductivity of $\text{Li}_3\text{V}_2(\text{PO}_4)_3$ (2.4×10^{-7} S/cm at room temperature) [22-25]. However, few researches have been

focused on the Li ion diffusion enhancement using this architecture to improve the high-rate and long-life performance of this material [26, 27].

Here, we describe a feasible method by decomposing the microflower precursor to prepare the nanoporous $\text{Li}_3\text{V}_2(\text{PO}_4)_3/\text{C}$ microspheres, which can provide fast Li ion and electron conduction. The obtained cathode material achieved an enhanced rate capability (112 mAh/g at rate up to 10 C, 1 C = 133 mA/g) and superior cycling stability (88% capacity retention after 500 cycles and 77% after 2000 cycles at the rate of 10 C).

2. Experimental Details

2.1. Material preparation

The nanoporous $\text{Li}_3\text{V}_2(\text{PO}_4)_3/\text{C}$ microspheres were synthesized by hydrothermal process combined with conventional solid-state method. Stoichiometric amounts of 0.01 mol vanadium pentoxide (V_2O_5) and oxalic acid ($\text{H}_2\text{C}_2\text{O}_4$) were dissolved into deionized water with stirring at 80^oC for 15 min (molar ratio of $\text{V}_2\text{O}_5/\text{H}_2\text{C}_2\text{O}_4=1:3$). After the formation of transparent solution of VOC_2O_4 , the phosphoric acid (H_3PO_4), lithium acetate (CH_3COOLi) were added into the above solution (molar ratio of Li: V: P = 3:2:3). 5 mL ethylene glycol (EG) was then added to the solution. And 5 mL anhydrous ethylenediamine (EN) was dropwise added to the solution after 30 min. Along with the addition of EN, tiny green precipitate appeared. After stirring for 2 h, the green suspended solution obtained above was transferred into a 100 mL Teflon-lined autoclave at 180^oC for 3 h. Afterwards, the precursor solution was dried at 120^oC in an air oven, followed by calcination at 350^oC for 5 h in nitrogen atmosphere to get a brown intermediate product. Finally, the brown powder was sintered at 800^oC for 8 h in nitrogen atmosphere to yield final

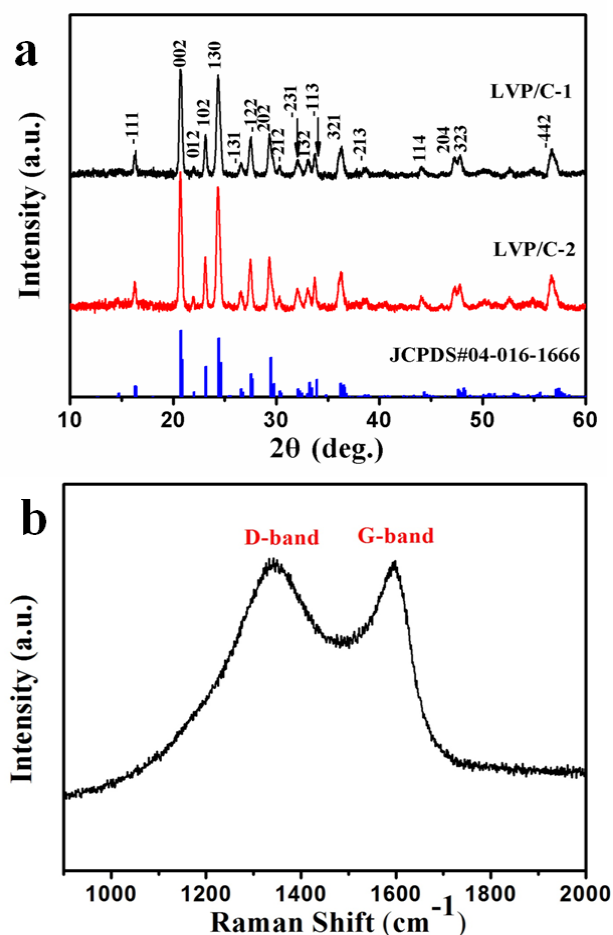


Figure 1. (a) XRD patterns of LVP/C-1 and LVP/C-2; (b) Raman scattering spectrum of LVP/C-1.

porous product, which is marked as LVP/C-1. For comparison, LVP/C-2 (non-porous) was also prepared using the same procedure without EN.

2.2. Material characterization

The crystal structures of LVP/C-1 and LVP/C-2 were confirmed by X-ray powder diffraction (XRD, Bruker D8 Advance) with non-monochromated Cu K α X-Ray source. The morphologies and element mappings of LVP/C-1 and LVP/C-2 were characterized by field emission scanning electron microscope (FESEM, JEOL JSM-7100F, 10 kV) and high-resolution transmission electron microscope (HRTEM, JEOL JEM-2100F, 200 kV). The specific surface area and Barrett-Joyner-Halenda (BJH) pore size distribution were analyzed using Micromeritics Tristar 3020 instrument. The property of carbon layer was analyzed with an INVIA Raman spectrometer.

2.3. Electrochemical tests

To make electrodes, 70% active materials were ground with 20% acetylene black and 10% poly(tetrafluoroethylene) (PTFE) to get circular disks with an average weight of 3 mg. CR2025 coin cells were assembled in a glove box filled with pure argon gas (O_2 and H_2O content < 1 ppm), using lithium pellets as the anodes and 1 M solution of $LiPF_6$ in ethylene carbon (EC)/dimethyl carbonate (DMC) as electrolyte. Before charging/discharging process, the cells were aged for 12 h to ensure full absorption of the electrolyte into the electrodes. Galvanostatic charging/discharging tests

were performed in the voltage range of 3.0 to 4.3 V at different current densities on a multichannel battery testing system (LAND CT2001A). The cells were charged under constant current and constant voltage (CCCV) mode, which was then discharged under constant current (CC) mode. The constant current charging is followed by a potentiostatic holding at 4.3 V until the current drops to 5% of charging current. The cells were then discharged to 3.0 V. Cyclic voltammetry (CV) test of cells was carried out with an electrochemical workstation (CHI 760D). The electrochemical impedance spectroscopy (EIS) was tested using another electrochemical workstation (Autolab PGSTAT 302N) at the cell voltage of 4.2 V in the frequency range 100 kHz to 0.01 Hz at 10 mV. All the tests were performed at room temperature.

3. Results and Discussion

The X-ray diffraction (XRD) patterns of LVP/C-1 and LVP/C-2 are shown as Figure 1a, which indicates that both samples exhibit good crystallinity and high purity without any secondary phases. Based on the XRD analysis, both materials are well indexed to the monoclinic $Li_3V_2(PO_4)_3$ (JCPDS Card no. 04-016-1666, space group P21/n). According to the elemental analysis results, the amount of carbon in LVP/C-1 and LVP/C-2 are about 9.97% and 2.80 %, respectively, which confirms that EN is an important carbon source. As shown in the Figure 1b, the Raman spectrum is dominated by two characteristic carbon signatures at 1342 and 1596 cm^{-1} , corresponding to the disorders or defects in the graphite structure (D-band) and the presence of the graphite carbon (G-band), respectively [11, 28, 29]. The value of the peak intensity ratio of the D to G band (I_D/I_G) is 1.01, indicating that the percentage of the graphite-like carbon fraction is 49.8% in the total carbon, which would result in an improved electrical conductivity [30].

FESEM image (Figure 2a) shows that the size of nanoporous LVP/C-1 microspheres is around 5-12 μm in diameter, which are comprised of smaller primary particles. Element mappings also show that C, V, P and O are distributed uniformly in the final product (Figure 2b). Without EN, the obtained LVP/C-2 microspheres are solid without the smaller primary particles and pores, which are clearly showed in Figure S1.

The nanoporous structure of LVP/C-1 microspheres is further evidenced by TEM image (Figure 2c). It is clear that LVP/C-1 microsphere is porous with clear void between nanoparticles, which are embedded in the carbon matrix (Figure 2d). The HRTEM image (Figure 2e) displays clear crystal lattice spacings of 0.36 and 0.43 nm, which match well with the separations between 130 and 002 planes of monoclinic $Li_3V_2(PO_4)_3$, respectively. And the single-crystalline nanoparticles are coated with amorphous carbon layer. The N_2 adsorption-desorption isotherms and the corresponding pore-size distributions are shown in Figure 2f. The nanoporous LVP/C-1 microspheres present type-IV adsorption-desorption isotherm with distinct H3-type hysteresis, a feature of mesoporous material [31]. Attributed to the mesoporous structure, LVP/C-1 microspheres show a high BET surface area of 61.9 m^2/g , which is much higher than 18.9 m^2/g of the non-porous LVP/C-2 (Figure S2).

A possible formation schematic of nanoporous LVP/C microsphere is shown in Figure 2g. EG is a common chelating agent to limit the particle growth and ensure the

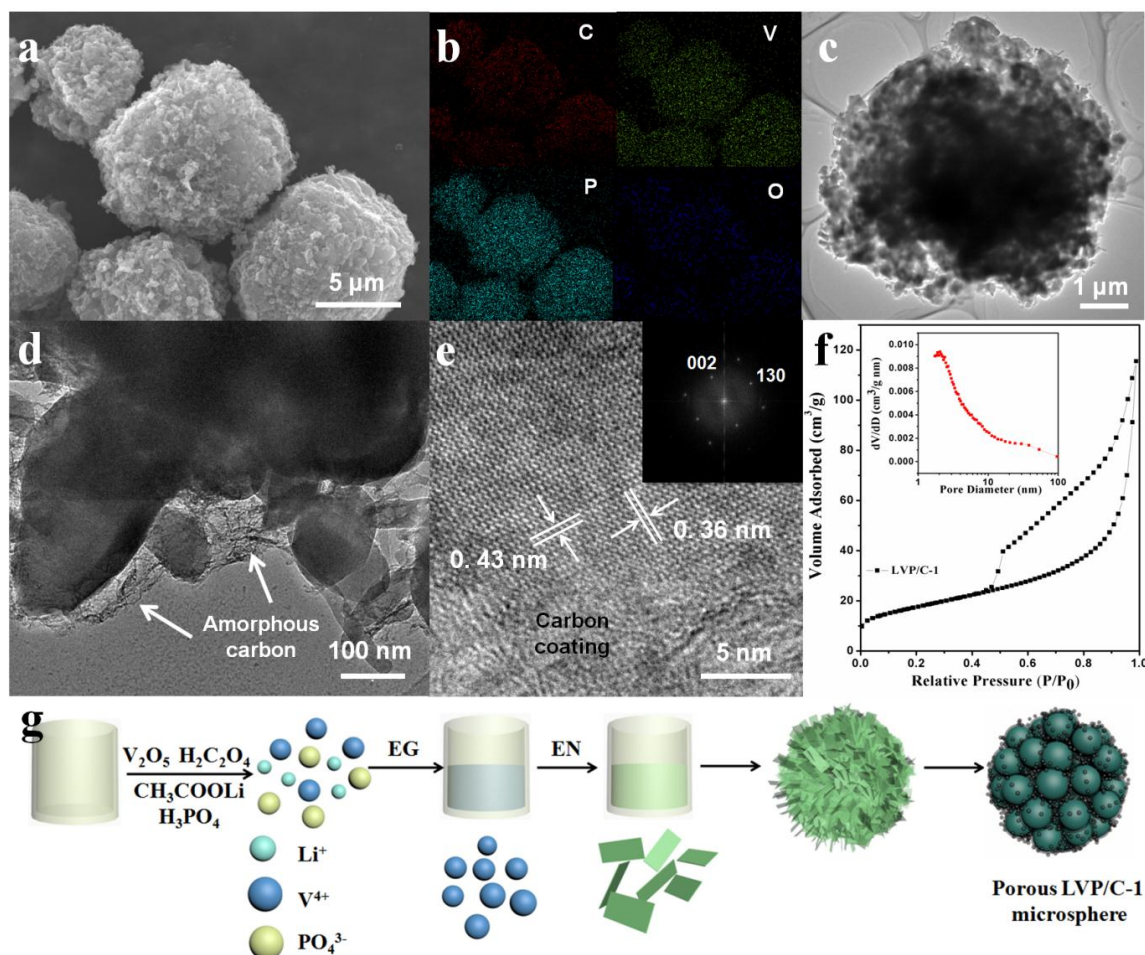


Figure 2. (a) Typical SEM image, and (b) EDX elemental mapping of LVP/C-1; (c, d) TEM, and (e) HRTEM images of LVP/C-1; (f) Nitrogen adsorption and desorption isotherms and pore size distribution (inset) of LVP/C-1 material; (g) Schematic illustration of the processes involved in the evolution of the nanoporous LVP/C-1 microsphere.

monodispersion of nanoparticles [4]. Li^+ and VO^{2+} cations are self-assembled to the EG by chelating effect to form the primary particles. As EN has a stronger chelating effect for VO^{2+} cations which may influence the release of isolated cations, the primary particles grow into green nanoplates due to van der Waals interactions [32]. Driven by minimization of total surface energy, these nanoplates would then aggregate into flower-like sphere precursor (Figure S3a-b and S4) [33]. After the thermal treatment under 800°C , the LVP/C microflower precursor were converted to the nanoporous microsphere owing to the release of gases in the thermal treatment process. In the control experiment in the absence of EN, the primary particle may aggregate into bigger particles during hydrothermal reaction without the stronger chelating effect of EN (Figure S3c-d), and then the non-porous LVP/C microspheres would form in the final high temperature processing (Figure S5).

Figure 3a shows the cyclic voltammograms (CV) of LVP/C-1 and LVP/C-2 cathode in the first cycle at a scan rate of 0.1 mV/s between 3.0 and 4.3 V vs. Li/Li^+ . It is obviously that LVP/C-1 have sharper peaks with higher redox currents, indicating an alleviated polarization and faster kinetics for Li ions insertion/extraction [11]. The CV curve of LVP/C-1 is taken to explain the electrochemical process. During the charging process, three well-defined oxidation peaks are observed at 3.62 , 3.70 and 4.13 V , respectively. The peaks at 3.62 and 3.70 V present the first lithium extraction from

$\text{Li}_3\text{V}_2(\text{PO}_4)_3$, which corresponds to ordered phases $\text{Li}_{2.5}\text{V}_3(\text{PO}_4)_3$ and $\text{Li}_2\text{V}_3(\text{PO}_4)_3$ ($\text{Li}_3\text{V}_2(\text{PO}_4)_3 \Leftrightarrow \text{Li}_{2.5}\text{V}_2(\text{PO}_4)_3 \Leftrightarrow \text{Li}_2\text{V}_2(\text{PO}_4)_3$) with a mixed-valence $\text{V}^{3+}/\text{V}^{4+}$, respectively. The peak located 4.13 V is related to the delithiation of the second Li to form $\text{LiV}_2(\text{PO}_4)_3$ ($\text{Li}_2\text{V}_2(\text{PO}_4)_3 \Leftrightarrow \text{LiV}_2(\text{PO}_4)_3$), which corresponds to the complete oxidation of V^{3+} to V^{4+} [34, 35]. The peaks at 3.51 , 3.59 and 4.0 V in the discharging process correspond to the reversible insertion of extracted Li ions. Figure 3b compares the charging/discharging plateaus of LVP/C-1 and LVP/C-2 at 0.5 C . For LVP/C-1, three plateaus located around 3.64 , 3.70 and 4.09 V can be well identified as the extraction of lithium ions and the corresponding phase transition process during the electrochemical reactions. Meanwhile, during the discharging process, three plateaus located around 4.04 , 3.63 and 3.54 V can be attributed to the insertion of the extracted Li ions, which is accompanied the phase transition from $\text{LiV}_2(\text{PO}_4)_3$ to $\text{Li}_3\text{V}_2(\text{PO}_4)_3$. The locations of the plateaus are consistent with the CV results. The charging/discharging curves of LVP/C-1 at different rates are shown in Figure S6. The charging/discharging plateaus at 10 C are still apparent, although they become shorter gradually with the increase of the discharging rate.

In order to demonstrate the superior electrochemical performance of LVP/C-1 cathode, the initial discharge capacity and the capacity retention after 50 cycles at different rates of both samples are depicted in Figure 3c. LVP/C-1 cathode delivers a much higher initial discharge capacities of

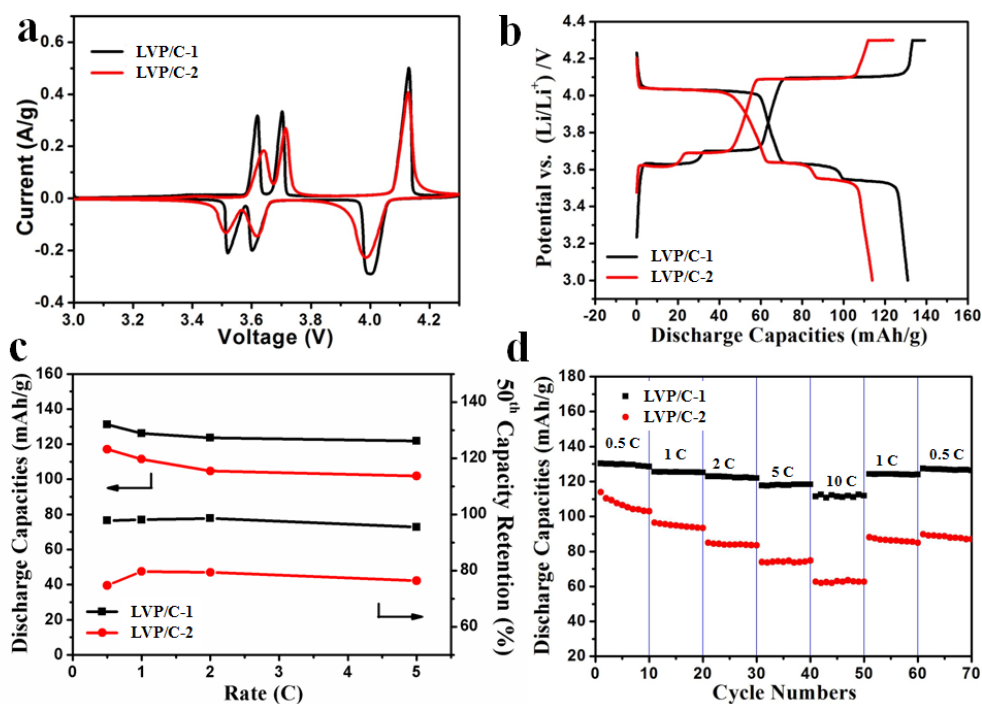


Figure 3. Electrochemical properties of LVP/C-1 and LVP/C-2. (a) CV curves at the scan rate of 0.1 mV/s in the voltage range from 4.3 to 3.0 V vs. Li/Li⁺. (b) The second charging/discharging curves of LVP/C-1 and LVP/C-2 at 0.5 C. (c) Comparison of the initial discharge capacities and the capacity retention after 50 cycles versus different discharging rates. (d) Rate performance of LVP/C-1 and LVP/C-2 cathode from 0.5 to 10 C.

131, 126, 124 and 122 mAh/g at the current densities of 0.5, 1, 2 and 5 C, respectively. The corresponding values of LVP/C-2 cathode are 117, 112, 105 and 102 mAh/g, respectively. More importantly, LVP/C-1 cathode exhibits better cycling performance as the corresponding retentions are 98%, 98%, 99% and 96% after 50 cycles at the above rates, which are much higher than 75%, 80%, 79% and 76% for LVP/C-2, respectively. The detailed cycling performances of both samples at different rates are shown in Figure S7. To eliminate the influence of different carbon content in LVP/C-1 and LVP/C-2, more carbon black is added in LVP/C-2 to get the same carbon content with LVP/C-1. However, even in this case, the capacity increase of LVP/C-2 cathode with extra carbon is smaller than 5 mAh/g compared to the regular one throughout the 100 cycles at 5 C, indicating that the porous morphology is the key point to achieve the superior electrochemical performance for LVP/C-1 (Figure S8).

The rate performances of LVP/C-1 and LVP/C-2 are shown in Figure 3d. The cells were cycled continuously at various rates and both cathode exhibit good rate response. Remarkably, even after 40 cycles, the LVP/C-1 still obtains a capacity of 111 mAh/g at 10 C and further test at 0.5 C brings the capacity back to 127 mAh/g, almost no capacity loss compared to the initial test. The capacity of LVP/C-2 decreases significantly with increasing rates. When the rate increases to 10 C, the sample only deliver a low capacity of 63 mAh/g, and the capacity recovery is also not desirable. The specific discharge capacity of the nanoporous Li₃V₂(PO₄)₃/C microspheres is much higher than that of the carbon coated Li₃V₂(PO₄)₃ cathode material prepared by a polyvinyl alcohol (PVA) assisted sol-gel method, which presents a capacity of 100 mAh/g at 1 C rate [36]. The monoclinic Li₃V₂(PO₄)₃ nanobelts demonstrate a high specific discharge capacity of 131 mAh/g and stable cycling characteristics. However, the

capacities at high rates are not satisfactory (110 mAh/g at 8 C rate) [13]. A facile sol-gel approach combined with a carbon-coating technique is also applied for the synthesis of a Li₃V₂(PO₄)₃/C cathode material. Although this material demonstrates a good cycling performance, it only delivers a reversible capacity of 107 mAh/g at 5 C rate [37]. These comparison results indicate that the nanoporous LVP/C-1 cathode material is one of the most attractive cathodes for the practical applications.

The detailed electrochemical reactions and Li ion diffusion processes of the LVP/C cathodes were investigated using EIS at the cell voltage of 4.2 V. It is clear that both of the Nyquist plots are composed of two arcs at high and middle frequencies, combined with a slanted line in the low-frequency region (Figure 4a) [38]. The arc centered at high frequency can be attributed to the contact resistance between the active materials and the substrate, combined with the double-layer capacitance created by the conductive substrate and the electrolyte. The latter arc indicates the charge transfer resistance coupled with the double-layer capacitance between the active material and the electrolyte. And the slanted line corresponds to the ion diffusion in the active material [39]. The fitted charge transfer resistance (R_{ct}) of LVP/C-1 and LVP/C-2 are 70 and 160 Ω , respectively. It is easily understandable that the charge resistance of LVP/C-1 is much lower as it has a much higher effective surface area and higher carbon content, which is beneficial for the electron conduction and lithium migration [40]. The slanted line corresponds to the ion diffusion in the active material. The lithium ion diffusion coefficient can be calculated from the plots in the low frequency region using Eq. 1, where R is the gas constant, T is the temperature, A is the area of the electrode surface, n is the number of electrons per molecule during oxidization, F is Faraday's constant (96486 C/mol), C is the molar

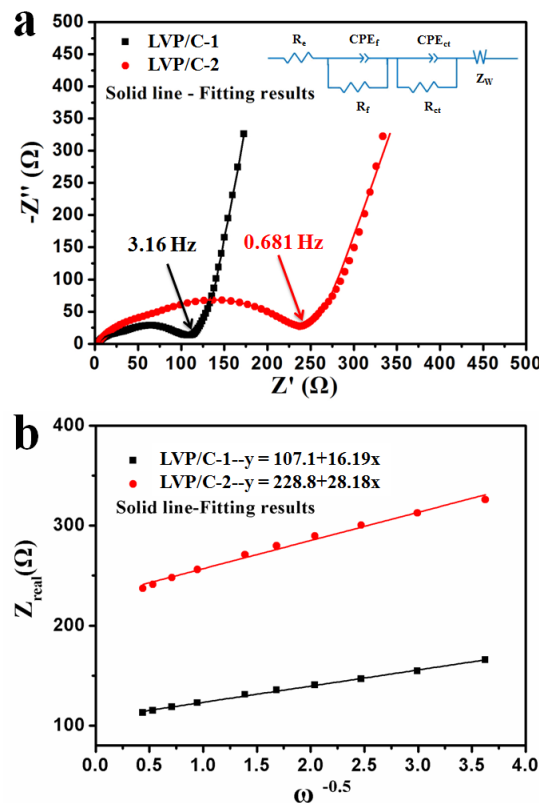


Figure 4. EIS plots of LVP/C-1 and LVP/C-2. (a) Nyquist plots, and (b) the plots of impedance as a function of the inverse square root of angular frequency in the Warburg region.

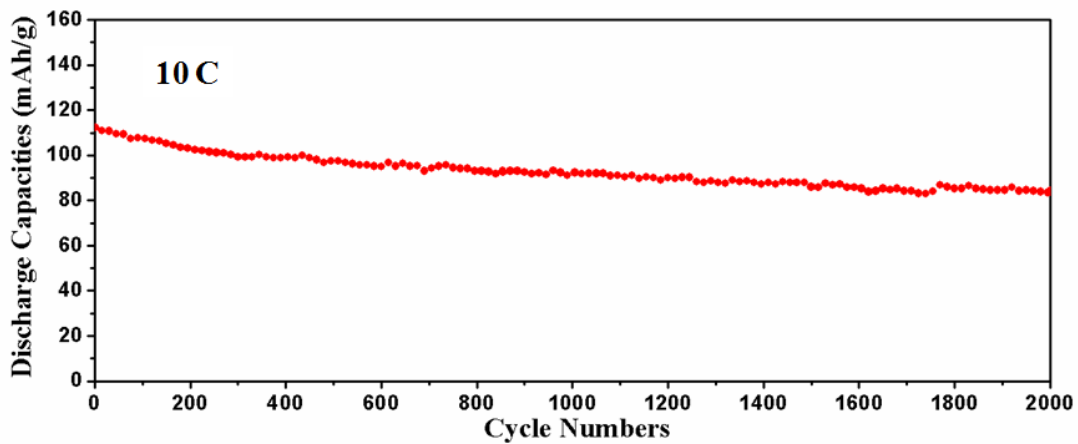


Figure 5. Cycling performance of LVP/C-1 at a high rate of 10 C for 2000 cycles.

concentration of Li^+ ions in the structure, and σ_w is the Warburg coefficient, which can be obtained from the slope of Z_{real} vs. $\omega^{-1/2}$ (ω is the angular frequency) in the Warburg region (Figure 4b) by Eq. 2.

$$D_{\text{Li}} = 0.5(RT/An^2F^2C\sigma_w)^2 \quad (1)$$

$$Z_{real} = R_e + R_f + R_{ct} + \sigma_w\omega^{-1/2} \quad (2)$$

When the cathode was charged to 4.2 V, two lithium would be extracted from the $\text{Li}_3\text{V}_2(\text{PO}_4)_3$ to form $\text{LiV}_2(\text{PO}_4)_3$ with a cell volume of 0.8251 nm^3 [7]. As a result, the value of C is $1.212 \times 10^{-3} \text{ mol/cm}^3$. Based on the equation mentioned above, the calculated D_{Li} for LVP/C-1 and LVP/C-2 are 2.28×10^{-10} and $7.53 \times 10^{-11} \text{ cm}^2/\text{s}$, respectively. The electrolyte ion diffusion starts at 3.16 Hz for LVP/C-1 and 0.681 Hz for

LVP/C-2, respectively, indicating the more facile Li ions diffusion inside the active material for LVP/C-1. Based on the above results, we may come to the conclusion that the nanoporous microspheres structure of LVP/C-1 is beneficial for the Li^+ extraction/insertion from/in the active materials.

Figure 5 displays the long-life performance of LVP/C-1 cathode at the rate of 10 C. The initial specific discharge capacity is 112 mAh/g. The specific capacity decreases to 98 and 86 mAh/g after 500 and 2000 cycles, corresponding to the capacity retentions of 88% and 77%, respectively. The capacity fading per cycle throughout 2000 cycles is 0.014%. These results indicate that the nanoporous LVP/C-1 cathode material is a promising candidate for high-rate and long-life Li ion battery.

4. Conclusions

We have demonstrated the feasible hydrothermal process combined with the conventional solid sintering method to synthesize nanoporous $\text{Li}_3\text{V}_2(\text{PO}_4)_3/\text{C}$ microsphere cathode material. This architecture provides efficient and rapid pathways for both Li ion and electron transport. A specific capacity of 131 mAh/g can be obtained at 0.5 C. When the rate up to 10 C, an initial specific capacity of 112 mAh/g can be obtained and the corresponding capacity retentions can reach 88% after 500 cycles and 77% after 2000 cycles, respectively. The excellent rate capability and long lifespan make nanoporous $\text{Li}_3\text{V}_2(\text{PO}_4)_3/\text{C}$ microsphere a promising cathode for the lithium ion batteries. In view of the facility during synthesis, the synthetic strategy could also be extended to other cathode and anode materials.

Acknowledgements

This work was supported by the National Basic Research Program of China (2013CB934103, 2012CB933003), the International Science & Technology Cooperation Program of China (2013DFA50840), National Natural Science Foundation of China (51072153, 51272197). Thanks to Prof. C. M. Lieber of Harvard University and Prof. Dongyuan Zhao of Fudan University for strong support and stimulating discussion.

References

1. M. Armand, J.-M. Tarascon, *Nature* 451 (2008) 652.
2. J.-M. Tarascon, M. Armand, *Nature* 414 (2001) 359.
3. A. S. Aricò, P. Bruce, B. Scrosati, J.-M. Tarascon, W. Van Schalkwijk, *Nat. Mater.* 4 (2005) 366.
4. C. W. Sun, S. Rajasekhara, J. B. Goodenough, F. Zhou, *J. Am. Chem. Soc.* 133 (2011) 2132.
5. N. Li, Z. Chen, W. Ren, F. Li, H.-M. Cheng, *Proc. Natl. Acad. Sci. U. S. A.* 109 (2012) 17360.
6. H. G. Zhang, X. D. Yu, P. V. Braun, *Nat. Nanotechnol.* 6 (2011) 277.
7. H. Huang, S. C. Yin, T. Kerr, N. Taylor, L. F. Nazar, *Adv. Mater.* 14 (2002) 1525.
8. X. Wang, X. Cao, L. Bourgeois, H. Guan, S. Chen, Y. Zhong, D. M. Tang, H. Li, T. Zhai, L. Li, *Adv. Funct. Mater.* 22 (2012) 2682.
9. C. Wang, H. M. Liu, W. S. Yang, *J. Mater. Chem.* 22 (2012) 5281.
10. L. Q. Mai, S. Li, Y. F. Dong, Y. L. Zhao, Y. Z. Luo, H. M. Xu, *Nanoscale* 5 (2013) 4864.
11. W. C. Duan, Z. Hu, K. Zhang, F. Y. Cheng, Z. L. Tao, J. Chen, *Nanoscale* 5 (2013) 6485.
12. A. Q. Pan, J. Liu, J. G. Zhang, W. Xu, G. Z. Cao, Z. M. Nie, B. W. Arey, S. Q. Liang, *Electrochem. Commun.* 12 (2010) 1674.
13. Q. Pan, D. W. Choi, J. G. Zhang, S. Q. Liang, G. Z. Cao, Z. M. Nie, B. W. Arey, *J. Power Sources* 196 (2011) 3646.
14. X. H. Rui, N. Ding, J. Liu, C. Li, C. H. Chen, *Electrochim. Acta* 55 (2010) 2384.
15. J. J. Wang, X. L. Sun, *Energy Environ. Sci.* 5 (2012) 5163.
16. L. Chang, L. Q. Mai, X. Xu, Q. Y. An, Y. L. Zhao, D. D. Wang, X. Feng, *RSC Adv.* 3 (2013) 1947.
17. L. F. Shen, C. Z. Yuan, H. J. Luo, X. G. Zhang, K. Xu, Y. Y. Xia, *J. Mater. Chem.* 20 (2010) 6998.
18. G. Zhou, D.-W. Wang, L. Li, N. Li, F. Li, H.-M. Cheng, *Nanoscale* 5 (2013) 1576.
19. X. C. Tian, X. Xu, L. He, Q. L. Wei, M. Y. Yan, L. Xu, Y. L. Zhao, C. C. Yang, L. Q. Mai, *J. Power Sources* 255 (2014) 235.
20. Y. Xia, Z. Xiao, X. Dou, H. Huang, X. H. Lu, R. J. Yan, Y. P. Gan, W. J. Zhu, J. P. Tu, W. K. Zhang, X. Y. Tao, *ACS Nano* 7 (2013) 7083.
21. S. M. Xu, C. M. Hessel, H. Ren, R. B. Yu, Q. Jin, M. Yang, H. J. Zhao, D. Wang, *Energy Environ. Sci.* 7 (2014) 632.
22. Deng, S. Zhang, S. Y. Yang, Y. Gao, B. Wu, L. Ma, B. L. Fu, Q. Wu, F. L. Liu, *J. Phys. Chem. C* 115 (2011) 15048.
23. Pei, Z. Q. Jiang, W. X. Zhang, Z. H. Yang, A. Manthiram, *J. Power Sources* 239 (2013) 475.
24. R. V. Hagen, A. Lepcha, X. F. Song, W. Tyrra, S. Mathur, *Nano Energy* 2 (2013) 304.
25. L. L. Zhang, G. Liang, G. Peng, Y. H. Huang, L. Wang, L. Qie, M. C. Croft, A. Ignatov, J. B. Goodenough, *J. Electrochem. Soc.* 159 (2012) A1573.
26. L. Zhang, H. F. Xiang, Z. Li, H. H. Wang, *J. Power Sources* 203 (2012) 121.
27. X. Y. Du, W. He, X. D. Zhang, Y. Z. Yue, H. Liu, X. G. Zhang, D. D. Min, X. X. Ge, Y. Du, *J. Mater. Chem.* 22 (2012) 5960.
28. Y. S. Chen, D. Zhang, X. F. Bian, X. F. Bie, C. Z. Wang, F. Du, M. Jang, G. Chen, Y. J. Wei, *Electrochim. Acta* 79 (2012) 95.
29. J. L. Yang, J. J. Wang, Y. J. Tang, D. N. Wang, X. F. Li, Y. H. Hu, R. Y. Li, G. X. Liang, T.-K. Sham, X. L. Sun, *Energy Environ. Sci.* 6 (2013) 1521.
30. Y. Q. Qiao, J. P. Tu, X. L. Wang, C. D. Gu, *J. Power Sources* 199 (2012) 287.
31. Y. L. Zhao, L. Xu, L. Q. Mai, C. H. Han, Q. Y. An, X. Xu, X. Liu, Q. J. Zhang, *P Natl Acad. Sci. USA* 109 (2012) 19569.
32. L. Hu, H. Zhao, X. R. Zheng, Y. M. Huang, P. Zhang, Q. W. Chen, *Sci. Rep.* 2 (2012) 986.
33. Q. Q. Xiong, J. P. Tu, Y. Lu, J. Chen, Y. X. Yu, Y. Q. Qiao, X. L. Wang, C. D. Gu, *J. Phys. Chem. C* 116 (2012) 6495.
34. W. Yuan, J. Yan, Z. Y. Tang, O. Sha, J. M. Wang, W. F. Mao, L. Ma, *J. Power Sources* 201 (2012) 301.
35. L. L. Zhang, G. Liang, G. Peng, F. Zhou, Y. H. Huang, M. C. Croft, A. Ignatov, *J. Phys. Chem. C* 116 (2012) 12401.
36. T. Jiang, W. C. Pan, J. Wang, X. F. Bie, F. Du, Y. J. Wei, C. Z. Wang, G. Chen, *Electrochim. Acta* 55 (2010) 3864.
37. J. Su, X. L. Wu, J. S. Lee, J. Kim, Y. G. Guo, *J. Mater. Chem. A* 1 (2013) 2508.
38. H. X. Ji, L. L. Zhang, M. T. Pettes, H. F. Li, S. S. Chen, L. Shi, R. Piner, R. S. Ruoff, *Nano Lett.* 12 (2012) 2446.
39. X. L. Wu, Y. G. Guo, J. Su, J. W. Xiong, Y. L. Zhang, L. J. Wan, *Adv. Energy Mater.* 3 (2013) 1155.
40. J. S. Luo, X. H. Xia, Y. S. Luo, C. Guan, J. L. Liu, X. Y. Qi, C. F. Ng, T. Yu, H. Zhang, H. J. Fan, *Adv. Energy Mater.* 3 (2013) 737.

Cite this article as:

Yanzhu Luo *et al.*: Nanoporous $\text{Li}_3\text{V}_2(\text{PO}_4)_3/\text{C}$ microspheres with enhanced lithium ion diffusion for high-rate and long-life lithium ion batteries. *Sci. Lett.* 2015, 4: 130